Geophys. J. Int. (2000) **140,** 71–82

Constructing synthetics from deep earth tomographic models

Sidao Ni, Xiaoming Ding and Don V. Helmberger
Seismological Laboratory, Caltech, 252-21 *Pasadena,* CA 91125, *USA. E-mails: stone@gps.caltech.edu; helm@gps.caltech.edu*

Accepted 1999 August 5. Received 1999 August 2; in original form 1998 December 21

SUMMARY

Recent studies of deep mantle structure indicate strong heterogeneity. To conduct high-resolution waveform modelling of these structures, we have developed a new method to construct 2-D synthetics directly from block-style tomographic models. Unlike the WKBJ approximation, which utilizes rays overshooting and undershooting receivers, our method (WKM approximation) uses rays that arrive at the receiver. First, the ray paths from the 1-D layered reference model are used to localize each ray segment, where the anomalous velocities are applied by overlay, as in tomography. Next, new p_i (t_i) (p_i ray parameter, t_i traveltime) are computed to satisfy Snell's law along with their numerical derivative ($\delta p/\delta t$), which is used to construct a synthetic seismogram similar to the WKBJ method. As a demonstration of the usefulness of this method, we generated WKM synthetics for the D'' region of high velocities beneath Central America based on Grand's tomography model. Reasonable fits to broad-band data are obtained by condensing his distributed anomalies into his lowermost mantle layer; such a 2-D model predicts synthetics containing a laterally varying S_{cd} triplication similar to observations.

Key words: D″, lateral heterogeneity, synthetic waveforms, tomography.

1 INTRODUCTION

Recent studies of lower mantle structure have revealed strong heterogeneity at scales from 10 to 10 000 km and velocity variations of up to 50 per cent in extreme situations (see review in Lay *et al.* 1998). Long-period global studies display a circum-Pacific pattern of normal velocities with embedded high-velocity structures, particularly beneath eastern Asia and the Caribbean. The mid-Pacific is relatively slow, with very low velocities within specific regions (Wen & Helmberger 1998; Breger & Romanowicz 1998; Breger *et al.* 1998). Some of the high-velocity pockets seen in traveltime tomography are underlain by sharp features that can produce triplications. Lay & Helmberger (1983) employed several 1-D *S*-velocity models (Fig. 1) to explain some of these observations. In these models, the thickness of D″ varies considerably and has been inferred to be 250 km (SLHA), 280 km (SLHO) and 320 km (SLHE). These models, although very simple, can fit about 90 per cent of their data. The basis for their differences is that the triplications, as displayed in Fig. 2, vary in position between *S* and S_cS from region to region, that is, points b and c are not global (Wysession *et al.* 1998). Moreover, there is considerable variation across any particular region, as shown by Weber *et al.* (1996) for the area beneath Asia (SLHE) and by Kendall & Nangini (1996) for the Caribbean (SLHA) region. The lateral variation associated with the triplication beneath America was noted in the initial report by Lay & Helmberger (1983), as displayed in Fig. 3. Note that FBC is located in eastern North America whilst EDM is in western North America (Fig. 14). Their waveforms show distinctly different interference patterns for events arriving from South America. It would be particularly useful to explain such variation from tomography-based models with some fine-scale adjustments, as proposed by Sidorin & Gurnis (1998). They demonstrated that the above S_{cd} triplication can be produced by a positive velocity gradient induced by subducted material superimposed on a small global velocity discontinuity of 1. Dynamic modelling suggests why this phenomenon is likely to be rapidly varying and 3-D in nature (Sidorin *et al.* 1998).

To retrieve this type of detail from seismology, we need to move beyond 1-D modelling and use 3-D tomographic models based on traveltime analysis as a starting point. In particular, we introduce a new method of generating synthetics directly from 2-D sections through these models so that local modifications can be made to explain regional features such as those displayed in Fig. 3. Generating synthetics for heterogeneous earth models has a long history, in which many useful methods have been developed (Aki & Richards 1980). For many applications, the WKBJ approximation proves particularly appealing (Chapman 1978). An application of the method to deep earth models is discussed by Chapman & Orcutt (1985) along with a comparison of 1-D synthetics generated with those generated by the FK method. The WKBJ method has been extended to two dimensions by Chapman & Drummond (1982), referred to as Maslov Theory. Graves & Helmberger (1988) applied this approach to modelling multiple *S* phases (*S*, *SS*, . . .) with some

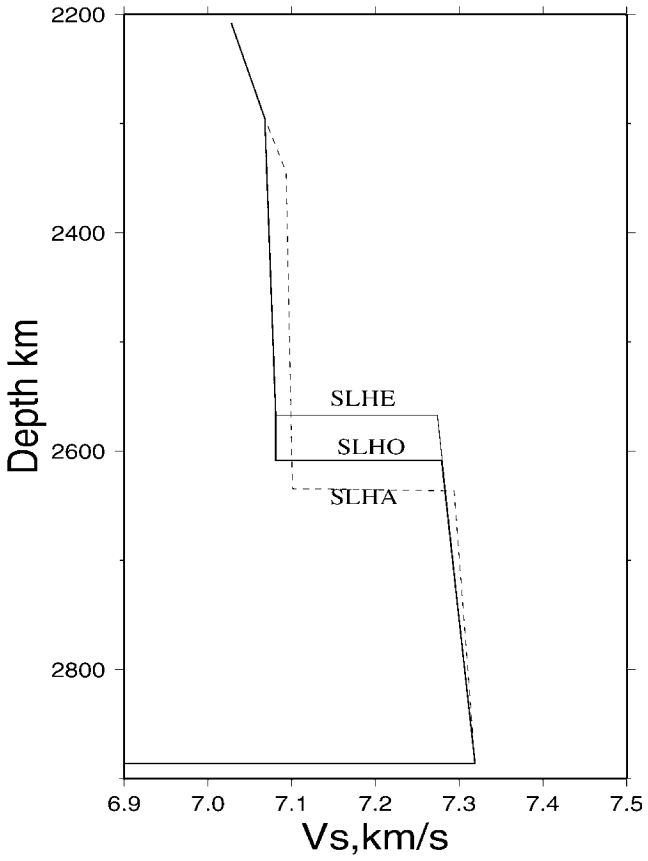

Figure 1. *S*-velocity models showing regional variation of D″ thickness. SLHA denotes the model beneath central America, SLHE denotes the model beneath Asia and SLHO denotes the model beneath Alaska. The basic feature is a 2.75 per cent velocity discontinuity. (After Lay & Helmberger 1983.)

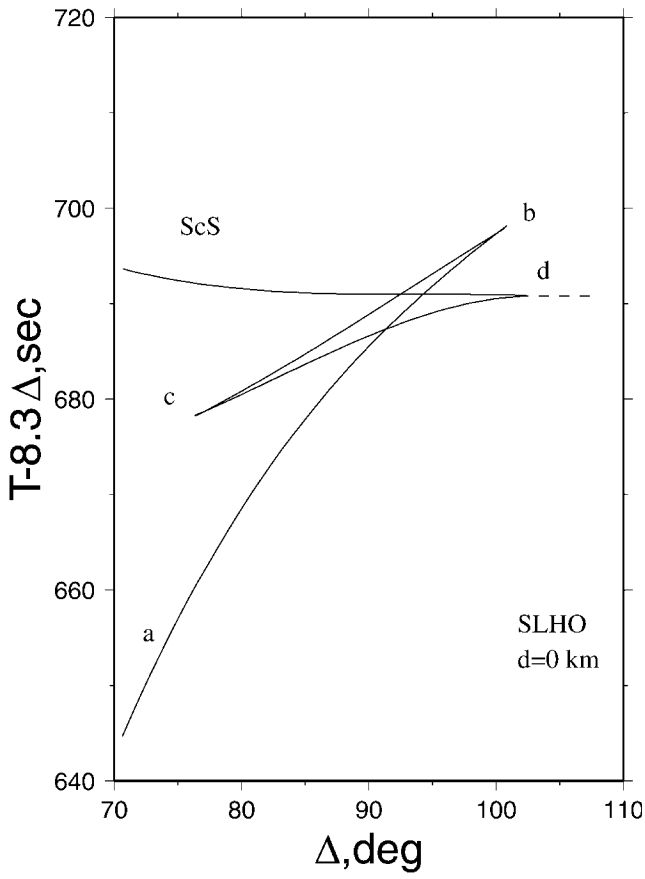

Figure 2. Triplication for the *S* phase (S_{cd}) together with S_cS, assuming a surface event for model SLHO. The cross-over distance shifts back for deeper sources, e.g. 85° for a 600 km deep source.

success. Liu *et al.* (1998) demonstrated that this method could produce D″ triplications from long-wavelength variations if they inflated the structural contrast of the Su *et al.* (1994) model, but no comparison of synthetics with data was presented.

Ding & Helmberger (1997) modelled a profile of broad-band S_{cd} data from the Californian arrays TERRAscope (Caltech) and BDSN (Berkeley Digital Seismography Network) and again found evidence for lateral variation on several scales. They presented synthetics for a possible 2-D model consisting of layers with varying thicknesses by applying a modified Cagniard–de Hoop approach (Helmberger *et al.* 1996). Here we introduce an approximate solution, WKM, to a layered block model, with constant layer thickness but varying velocity, and apply it to the Caribbean anomaly discussed above.

2 THE WKM APPROXIMATION

We begin with a brief review of the WKBJ method and its relationship to generalized ray theory (GRT) for a 1-D layered model. Fig. 4 displays the primary difference in ray path geometry for the simple turning-ray solution in a smoothly varying material, assumed to be a layered model. The WKBJ method can be derived directly from asymptotic theory (wavefront expansion) (Chapman 1978; Chapman & Drummond 1982) and is based on geometric ray paths of the type displayed in Fig. 4(b). The solution is constructed from a large number of rays arriving before and beyond the receiver. These rays have ray parameter (p_i) and traveltime (t_i). The wavefield at the receiver can be approximated with the summation

$$\sum_i \frac{p_i - p_{i-1}}{t_i - t_{i-1}} . \tag{1}$$

Following the GRT approach (Helmberger 1968), we sum generalized rays connecting the source to the receiver after reflecting from each layer interface, starting and ending with the rays displayed in Fig. 4(a). Chapman (1976) showed that the sum of these generalized rays can be replaced by a complex integration over depth and that this integral can again be approximated by expression (1). A similar solution was found by a numerical approximation of GRT synthetics (Wiggins 1976). The two solutions with similar expressions yield about the same synthetics (Helmberger *et al.* 1996) but have distinctly different ray paths. So as to avoid confusion, we will refer to methods involving the type of ray paths displayed in Fig. 4(a) as the WKM method. Also displayed in Fig. 4 is a low-velocity zone (LVZ) situated so as to demonstrate the differences in methods that can arise. WKM (a) utilizes rays arriving at the receiver and total responses are derived by summing the contribution from each ray, whilst WKBJ (b) uses rays overshooting and undershooting the receivers, which might potentially violate causality, as discussed by Burdick & Salvado (1986). They used the earlier approach (Chapman 1976) in their development of a 3-D slowness method.

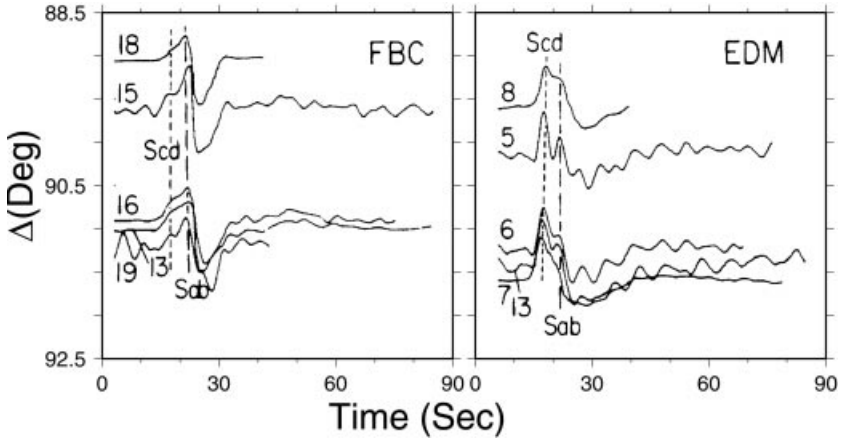

Figure 3. Long-period *SH* records at FBC (Frobisher Bay, Canada) and EDM (Edminton, Canada) for some events beneath South America. The traces are aligned on the first arrival. For FBC, S_{cd} is weaker than S_{ab}, whilst for EDM, S_{cd} is stronger than S_{ab}. (After Lay & Helmberger 1983).

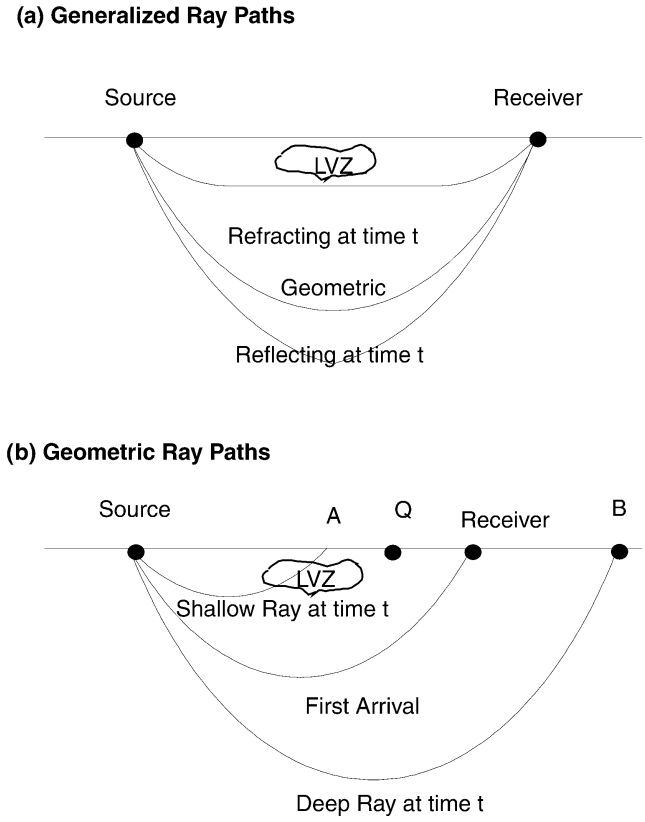

Figure 4. Two possible choices of ray paths for slowness calculations involving generalized ray paths and geometric ray paths. The generalized paths in (a) define a different envelope of causality from the geometric paths displayed in (b). In (a) the rays are generalized, each ray being reflected from each layer interface. The rays above the geometric ray carry refracted energy, whilst the rays below the geometric ray carry reflected energy. All the rays connect the source and receiver. WKM integrates the contribution of each ray to produce synthetics (see Fig. 6 for details). In (b) the rays are geometric rays; these rays overshoot or undershoot the receiver. The WKBJ method integrates all the contributions of these geometric rays to produce synthetics. The two sets of rays interact with perturbations in very different ways. (Modified from Burdick & Salvado 1986.)

Because WKBJ can be directly derived from classical optic theory, it proves relatively easy to treat 3-D problems for smoothly varying media (Liu & Tromp 1996). Sharp boundaries cause difficulties following this approach where GRT has some advantages. Energy trapping caused by locally dipping structure provides a good example where comparisons of GRT solutions with finite difference methods prove that GRT is quite good (Vidale & Helmberger 1988). Unfortunately, such solutions involve dealing with spatially dependent ray parameters and their attendant problems (Frazer & Phinney 1980). A simple example of locally dipping interfaces and how they have been treated is displayed in Fig. 5 (Hong & Helmberger 1978). The relationship between t_i and local ray

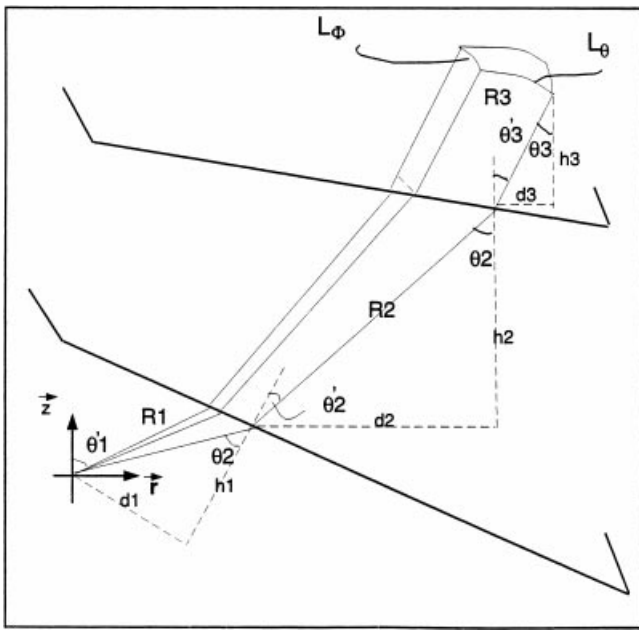

Figure 5. Diagram displaying geometrical spreading for locally dipping interfaces. The parametrization used in generating GRT synthetics is indicated in terms of d_i and h_i (after Hong & Helmberger 1978).

parameter p_i becomes

$$t = p_i d_i + h_i \left(\frac{1}{\beta_i^2} - p_i^2 \right)^{1/2}, \quad (2)$$

where β_i is the shear velocity and d_i and h_i are defined in Fig. 5. Changes in the ray parameter p caused by the dipping interfaces are embedded in p_i. Applying this procedure to a large number of layers is obviously cumbersome in the same way as computing synthetics in spherical shells (Gilbert & Helmberger 1972). In this case, the solution was simplified by adjusting the velocities to correct for changes in the relative slopes of interfaces, which leads to earth flattening.

Following this approach, Helmberger *et al.* (1996) introduced the local stretching approximation to 2-D structures that maps d_i, β_i and h_i from Fig. 5 into d_i', β_i' and h_i', where $p_i = p$ is constant along a ray path. Thus, the ray path displayed in Fig. 5 maps the dipping structures into a flat-layered model with the d_is lying along the interfaces and the h_is at right angles. Note that if the ray was reflected back through the layers, these parameters would take on different values. The accuracy of this approach is demonstrated in the above study by comparing

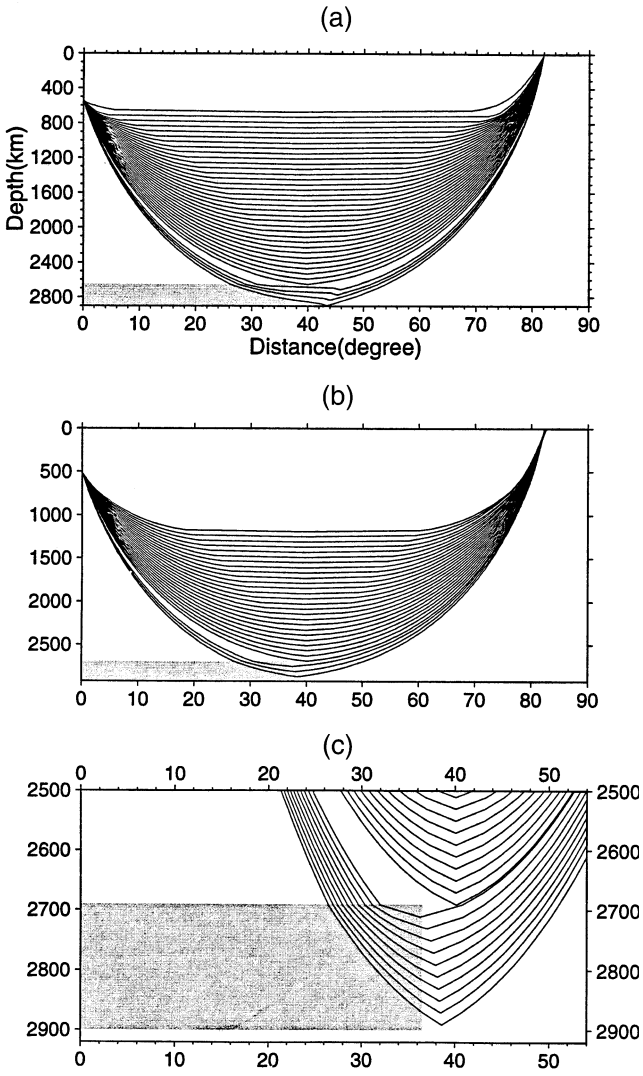

Figure 6. Ray paths connecting the various interfaces to the source and receivers at a distance of 82°. The shaded zone represents a 4 per cent increase in velocity relative to PREM (Dziewonski & Anderson 1981), where the anomaly extends from 0° to 36°. (a) displays these paths where the ray path does not bend when the effects of crossing the walls of the box have been neglected; (b) includes such bending; (c) shows an enlargement of the anomalous region where the bending is more obvious.

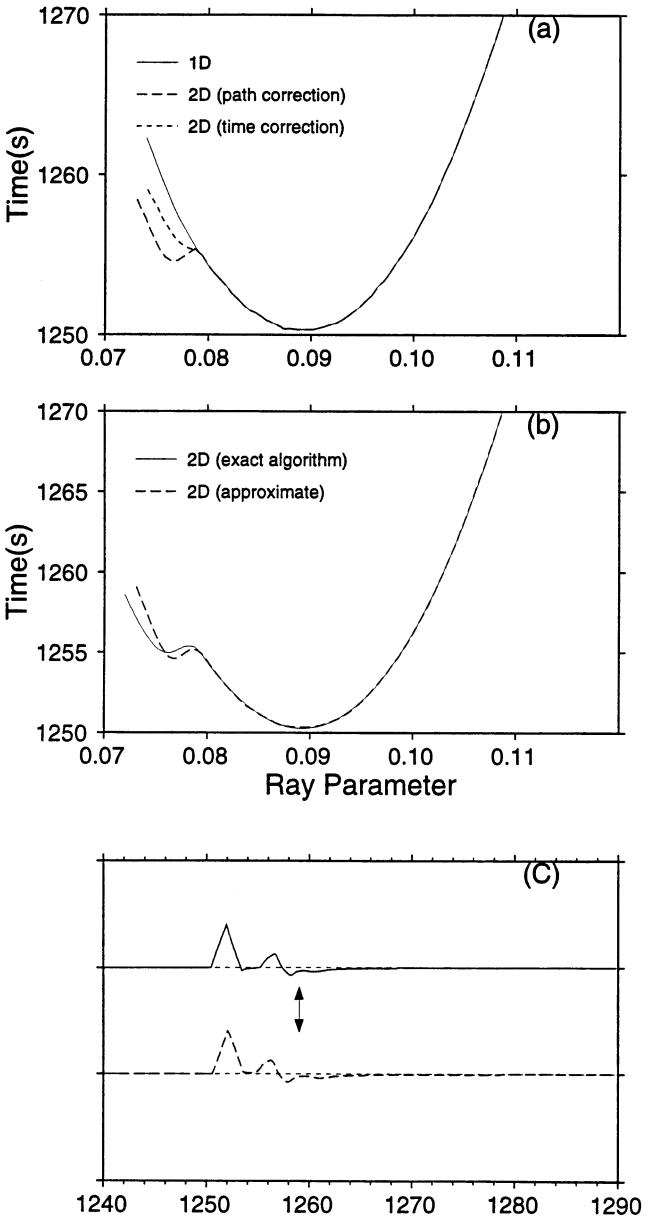

Figure 7. (a) $p-t$ curves for the three approximations for a distance of 82°. The solid curve is for the 1-D reference model (PREM). The dashed line is for the path-corrected approximation, where the faster zone flattens ray paths, causing a triplication, while 2-D time correction does not produce extra phases. (b) Approximate path correction versus exact path correction. The dashed curve is an approximate path-corrected $p-t$ curve and the solid curve is the $p-t$ curve for exact path correction, which is achieved by ray tracing to every interface by applying Snell's law. The approximate path correction is achieved by a local stretching algorithm assuming a constant layer velocity with no bending. (c) The synthetics based on the approximate path correction (dashed line) and exact path correction (solid). The arrows indicate the beginning of the truncation phase due to the existence of the CMB. The two seismograms show a very similar S_{cd} phase.

synthetics with the results of finite difference methods. A 2-D profile of synthetics generated with this code was presented in Ding & Helmberger (1997). Synthetics generated from such a parametrization have a natural relationship with block-style tomography models. Following the tomographic approximation, we find d_i, h_i and β_i for the 1-D reference model, we overlay a new velocity structure and we obtain d_i, β_i' and h_i, which freezes the path but will change the time. This scheme is used in most tomography studies and will be referred to as the time-corrected approach. A better approximation is to overlay the velocities and recompute the path d_i', β_i'. More accurate responses may be achieved in this way; we call this approximation path-corrected. Fig. 6 displays such paths for an earth-flattened model containing a fast block in D''.

Although this approach appears simple, the treatment of the vertical block boundaries needs to be addressed; in particular, the way we handle the ray bending that occurs when a ray crosses into a neighbouring block within a layer. In Fig. 6(a) the velocity β_i' is assigned when crossing from interface $(i-1)$ into (i); this value remains until interface $(i+1)$ is encountered. There is thus essentially no correction at vertical boundaries in each layer. In Fig. 6(b), the rays are bent to correct for wall-crossing. Ray paths for (b) satisfy reciprocity, while those in case (a) do not. An enlargement of the ray paths is displayed in Fig. 6(c), showing the slight adjustment in path when leaving the fast block. To determine these paths involves iteratively recomputing ray parameter p so that the ray arrives at the receiver; in particular, the ray satisfies Snell's law on all velocity boundaries, both horizontal and vertical. The drawback of this exact ray tracing method when applied to tomographic models is that the ray will not always arrive at the receiver because of the existence of the corners of blocks in tomographic models.

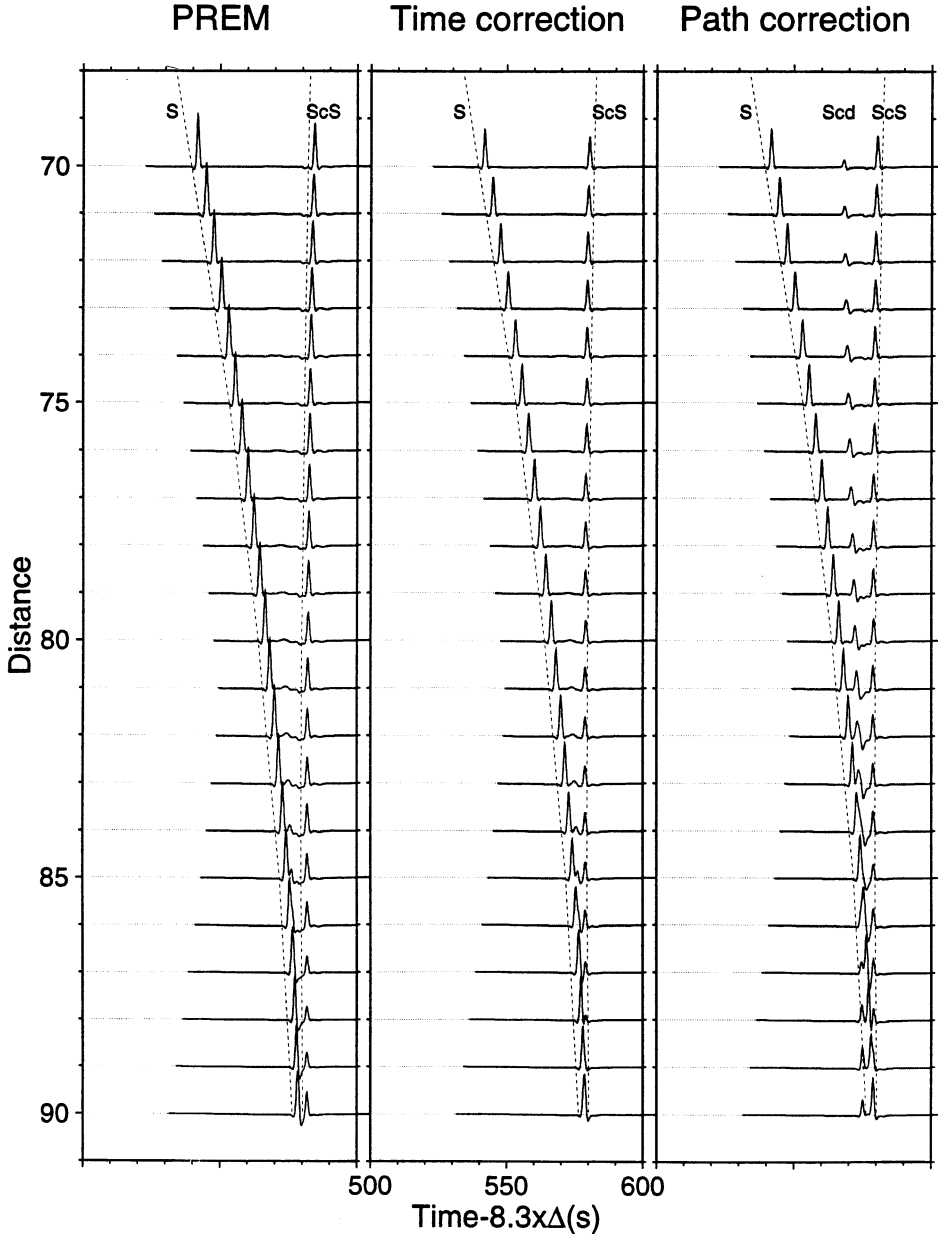

Figure 8. Synthetic record sections for one dimension, two dimensions time corrected and two dimensions path corrected. Traveltime is in reduced form. Note that the 2-D time correction synthetics do not show the S_{cd} phase but the 2-D path correction synthetics do.

Traveltime versus ray parameter plots ($t_i : p_i$) with these various approximations are displayed in Figs 7(a) and (b) for a distance of 82°. The PREM model (1-D) produces a smooth minimum that yields a simple square-root singularity for dp/dt, as expected for a geometric arrival (Chapman 1978). The time-corrected or tomographic approximation yields a slight secondary inflection, whilst the path-corrected approximation (Fig. 6a) produces a true secondary arrival or triplication, as can be seen in Fig. 8. The $t_i : p_i$ curves for a comparison of the two ray-tracing approaches discussed in Fig. 6 are given in Fig. 7(b). The two methods yield a small shift between S and the triplication, but with similar amplitudes. This particular example was computed assuming a layer thickness of 20 km, which produces about a quarter of a second offset in synthetics, as shown in Fig. 7(c). Decreasing the layer thickness reduces this offset, but this level of accuracy is equally affected by the choice of fitting a smooth curve through the discrete $t_i : p_i$ points needed in performing the derivative dp/dt. While a number of useful approximations are available (Chapman 1978), we found the generalized cross-validation (GCV) method (Wahba

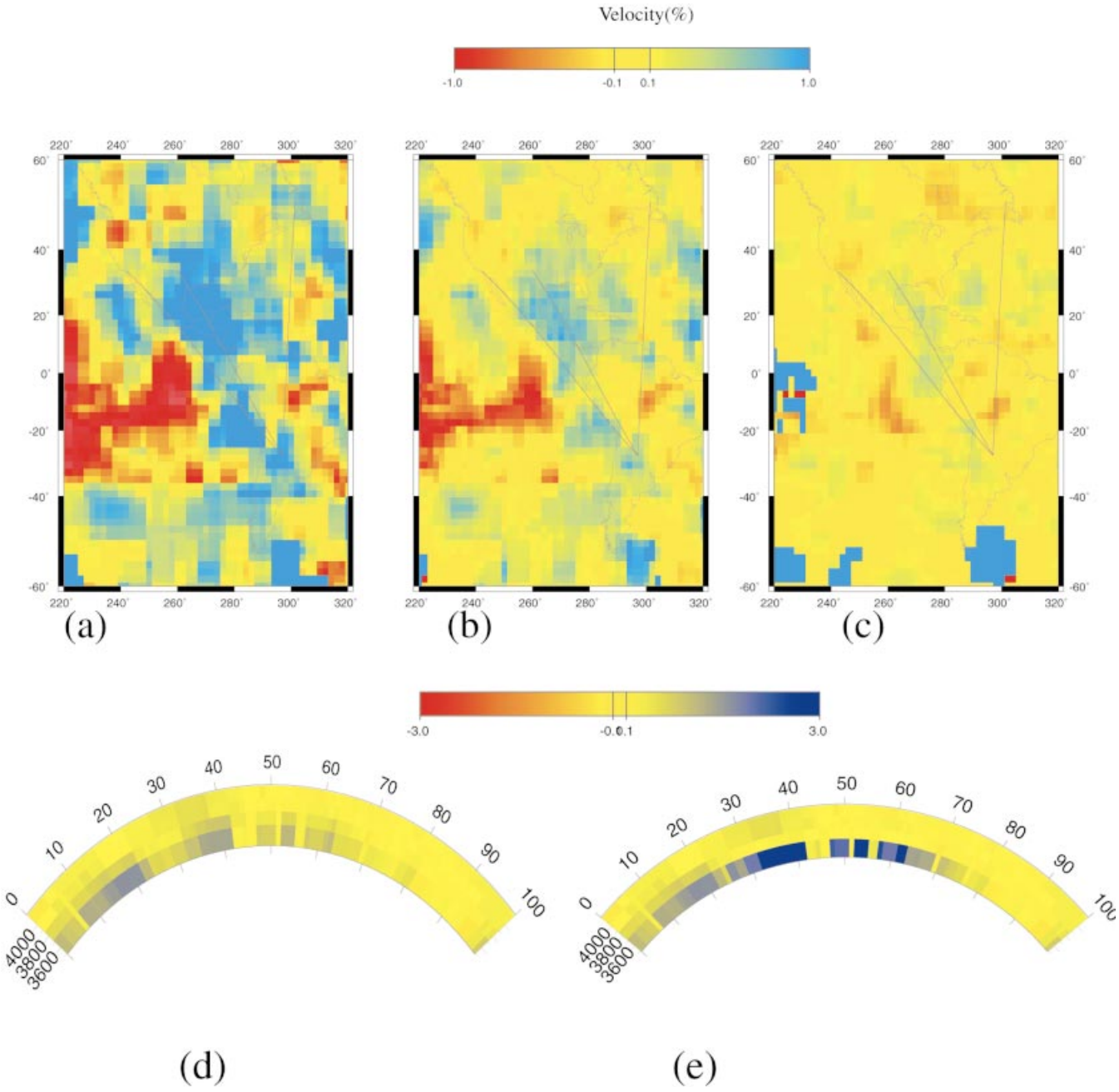

Figure 9. Horizontal slices of Grand's (1994) tomographic velocity model at three depths displaying the Caribbean anomaly: (a) 2890 (CMB)–2650 km, (b) 2650–2500 km, (c) 2500–2350 km. The three lines indicate azimuthal samples of the structure for an event located in Argentina (1994 October 5). The left line marks the western margin of the fast zone and the middle line marks the most anomalous portion. Note that the western region beneath the Caribbean is faster than the eastern region, which is the line marked on the right. (d) Grand's model. (e) Enhanced Grand's model, as described in the text.

1990) to be particularly effective. Basically, the GCV method minimizes simultaneously the integral of the square of the second derivative of the data and the variation between the data and the smoothed curve. Choosing cubic splines as a basis function $f(x)$, one can show that for a set of discrete data (x_i, y_i), $f_\lambda^{[k]}(x)$ minimizes

$$\frac{1}{n}\sum_{i\neq k}^{n}(y_i - f^{[k]}\lambda(x_i))^2 + \lambda\int_{x_0}^{x_n}(f''(x))^2 dx, \tag{3}$$

and λ is obtained by minimizing

$$V_0(\lambda) = \frac{1}{n}\sum_{k=1}^{b}(y_k - f_\lambda^{[k]}(x_k))^2 W_{kk}, \tag{4}$$

where W_{kk} is the weight for each data point, which is estimated automatically. For details, see Wahba (1990).

In summary, the distinction between the paths for approaches (a) and (b) of Fig. 6 disappears as the layer thickness is decreased, and neglecting ray bending at vertical boundaries circumvents the corner problem. Moreover, we do not expect such structures in the Earth and, neglecting corner diffractions is probably a reasonable approximation with respect to the usual determinations of tomographic models. In short, we will assume the simplified local stretching approximation where every ray path is obtained from a specific homogeneous layered velocity structure and can be easily determined.

The response for each of these rays can be generated following the GRT approach or we can obtain a useful WKM approximation, applying eq. (1) (Chapman 1976). The three sets of synthetics corresponding to the reference model and to the two approximations are shown in Fig. 8 following the latter method. The S_cS phase is shifted ahead about the same amount in both approximations relative to the PREM synthetics, since the S_cS path correction is less severe than for S_{cd}. The absence of the S_{cd} phase in time-corrected synthetics shows the necessity of performing the path corrections. Doubling the number of layers produces about the same synthetics, which is a good test of the procedure.

3 APPLICATION

Most tomographic models display relatively high velocities beneath Central America, including the inversion by Grand (1994), which we will use for demonstrative purposes (Fig. 9). This model displays a strong structural gradient beneath the Caribbean. Whilst the paths towards Newfoundland show a nearly PREM-like structure, the western paths cross major fast-velocity structures. This feature appears to be compatible with the observation of Kendall & Nangini (1996), who argued for strong variations in S_{cd} beneath the Caribbean (strong towards the west and weak toward the east).

However, Grand's model has a relatively smooth vertical D″ structure since this tomography model does not contain information about the S_{cd} phase. This can be seen in the 2-D cross-section displayed in Fig. 9(d) connecting Argentina to California. Synthetic predictions from this section are given in Fig. 10(a) with no noticeable S_{cd} phase. A modification is displayed in Fig. 9(e), where we follow Grand's (personal communication, 1998) suggestion of enhancing the anomalies in the lowermost layer by a factor of 3 whilst compensating in

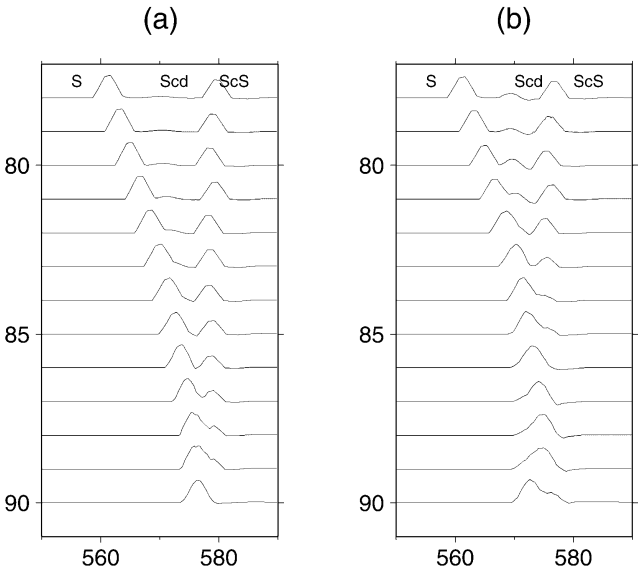

Figure 10. 2-D synthetics for (a) Grand's model and (b) the enhanced model. Before enhancement, Grand's model does not produce an appreciable S_{cd} phase, whilst the enhanced model does.

overlying layers. These modifications of tomography models are quite similar to the approach used to study traveltime and waveform anomalies (Ni *et al.* 1999) and have proved to be quite useful. This change artificially produces a triplication (S_{cd}) whilst roughly conserving the traveltime variations in S and its multiples, S_cS and SKS, which are used in the original tomographic model. Clearly, such a mapping is rather arbitrary and we will simply use it as one possible idealization and make synthetic predictions along various profiles. Note that these tomographic images are by their nature rough and some smoothing procedure should probably be applied, but at this stage of exploratory waveform imaging we will simply use them directly, although by omitting 'corners' we have *de facto* smoothed.

As discussed earlier, D″ appears to contain a broad range of structures on different scales. Thus, for our first numerical experiment we will revisit the broad-band California data studied by Ding & Helmberger (1997). A selection of data showing the S_{cd} phase is displayed in Fig. 11, along with synthetics from a 1-D subducted slab model proposed by Sidorin & Gurnis (1998). Their model contains a double thermal boundary layer, one at the CMB (negative gradient) and the other approaching a 1 per cent velocity jump (positive gradient) a couple of hundred kilometres above the CMB. Synthetics for the enhanced model clearly show S_{cd} phases (Fig. 11c). Although 1-D synthetics fit the traveltimes well, the amplitudes of the S_{cd} phases are too strong compared to the observed data at some stations, e.g. PAS. The 2-D synthetics fit the relative amplitude of S_{cd} to S at some stations, but do not fit the timing separation between S and S_cS as well as the 1-D model. This feature is easily accommodated by adding a low-velocity boundary layer approaching the CMB, as in Sidorin & Gurnis (1998). Perhaps a more interesting feature displayed by this observed record section is the rapid variation associated with S_{cd}. Note that S_{cd} appears early and strong at NEE whilst it is relatively weak and late at BAR; the pattern varies for different events (Ding & Helmberger 1997). We could alter the 2-D structure to increase

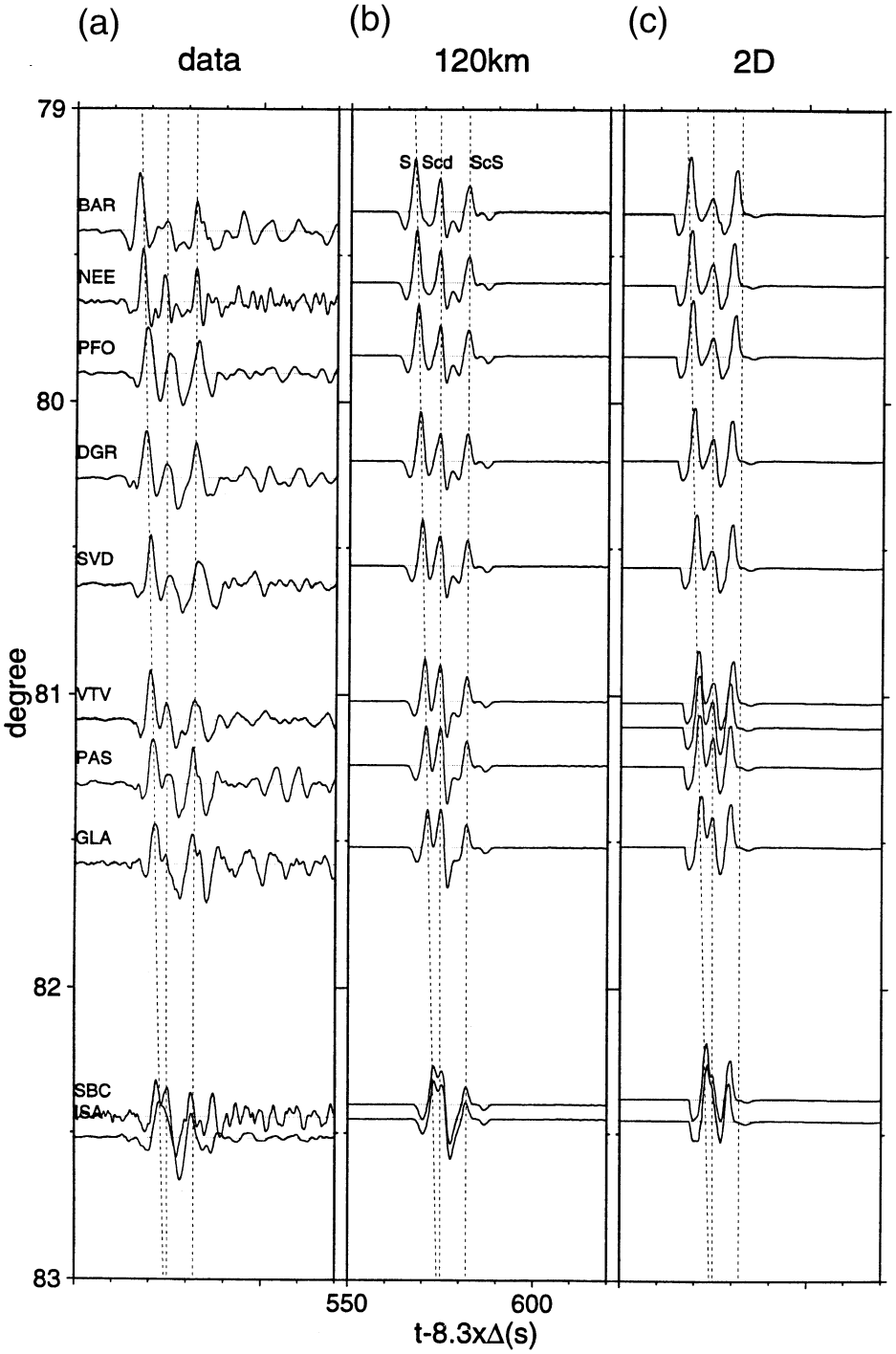

Figure 11. Comparison of waveform data with 1-D and 2-D synthetics. The data (*SH*) were recorded by TERRAscope stations for the Argentine event (1994 May 10) (Ding & Helmberger 1997). 1-D synthetics assume a 1-D model with a 120 km transitional zone 280 km above the CMB (see Sidorin & Gurnis 1998). 2-D synthetics are based on the enhanced model in Fig. 9(e).

the amplitude of S_{cd} and make it more variable, but for this to be meaningful would require extensive data analysis. This will be possible with the extended broad-band network installation now in progress (Jones *et al.* 1999)

Two synthetic record sections along the paths to FBC and EDM are displayed in Fig. 12. As expected, the FBC synthetics show a weak S_{cd} relative to S_{ab} because the structure is approaching PREM. These predictions can be compared with the observed data displayed in Fig. 3. Whilst these predictions do not overlie the observed waveforms exactly, they do compare quite well at a range of 88°–91° (Fig. 13). Note that the strong shoulder indicated by the second arrow in EDM lp matches the data. In contrast, the second arrival (S_{ab}) appears stronger in the FBC lp synthetics, which agrees with the data.

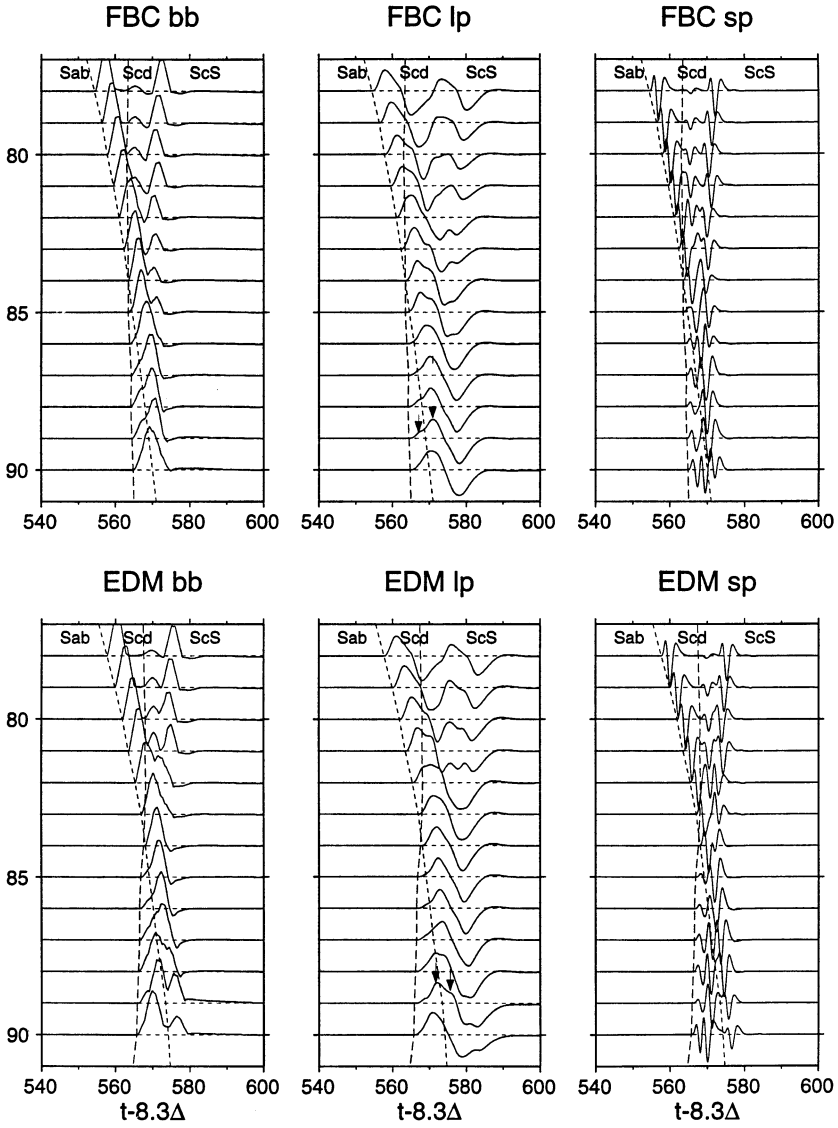

Figure 12. Synthetic profile along azimuths to FBC (top) and EDM (bottom). The left, middle and right panels are broad-band, WWSSN long-period and WWSSN short-period synthetics respectively; the WWSSN short-period synthetics are for comparison with the observations given in Lay & Helmberger (1983). On the broad-band synthetics, FBC shows a weak S_{cd} phase whilst EDM shows a strong S_{cd} phase relative to S_{ab}. Arrows mark the peaks of S_{cd} and S_{ab} on the long-period synthetics.

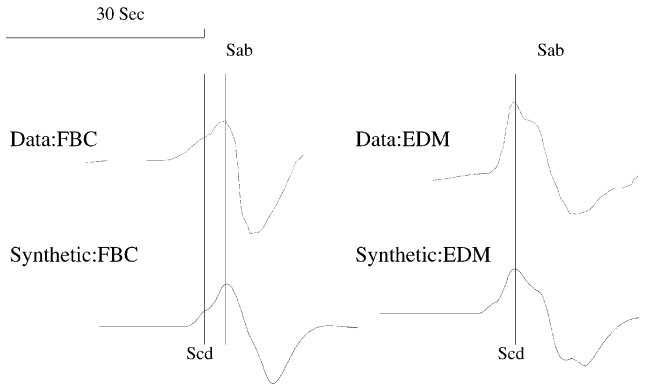

Figure 13. Data and synthetics for stations EDM and FBC. The data (top row) are for event 18 from Lay & Helmberger (1983) (see Fig. 3). The synthetics are those marked by arrows in Fig. 12 .

Lay & Helmberger (1983) also showed short-period observations at those ranges where EDM data clearly showed two arrivals similar to those in our synthetics. Thus, even though these waveform features appear subdued, they are probably observable, especially at distances greater than 90°, with the new broad-band data currently available and the new classes of D″ models recently introduced.

An overlay of the synthetics generated along the azimuths to EDM and FBC shows some interesting time-shifts. At the smallest ranges, the FBC records arrive about 6 s earlier than at EDM, as expected from the contrast in upper mantle structure (Grand & Helmberger 1984). However, at the largest ranges they have nearly the same arrival times because of the fast D″ structure along the EDM azimuth, which essentially compensates for the upper mantle delay. The cross-over distance shifts to smaller ranges for this reason. In the lower panel

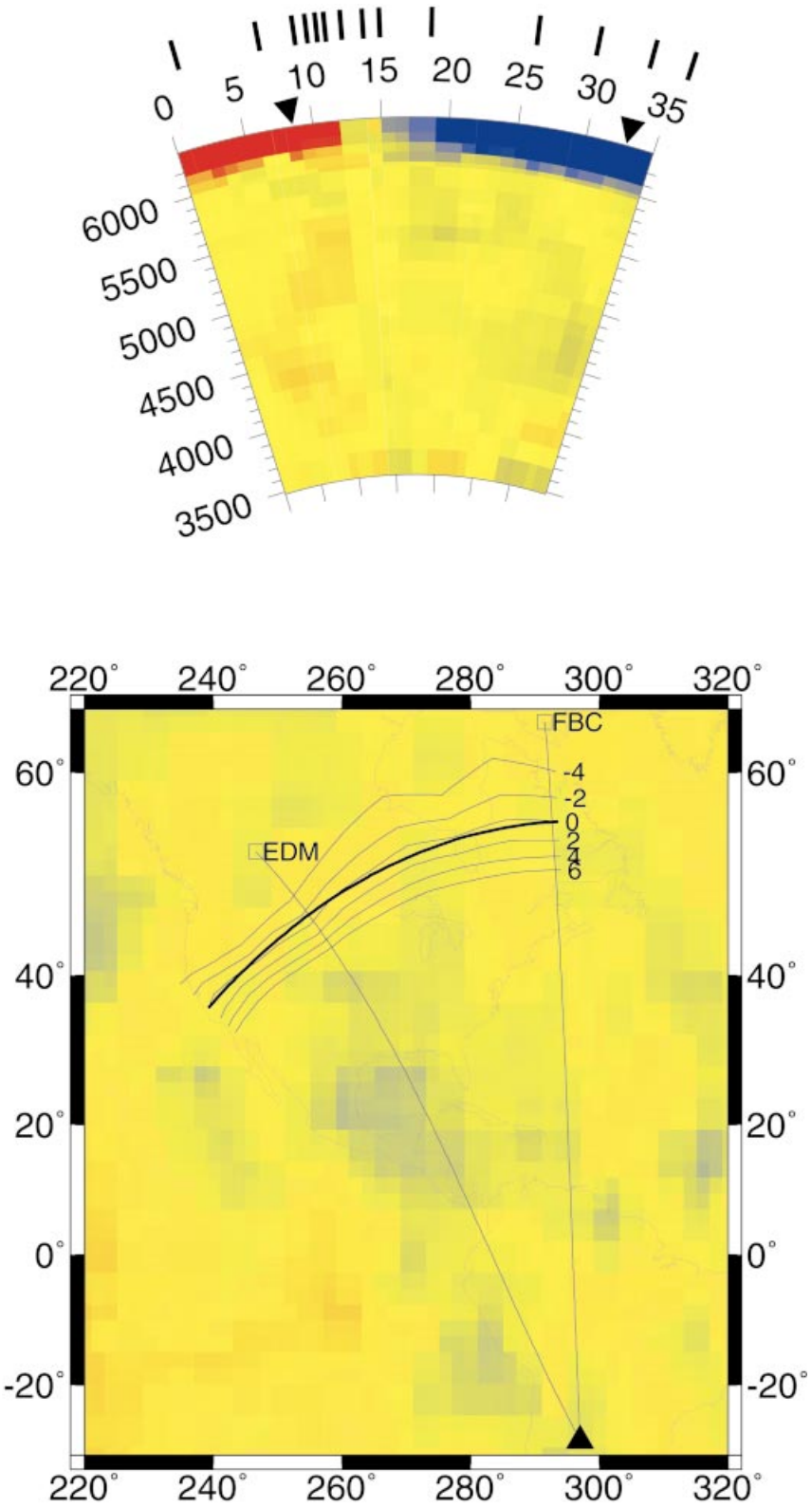

Figure 14. (a) Traveltime of S_{ab} obtained from 2-D synthetics along various azimuths. The velocity structure is from Grand's modified model and the cross-section is defined by the 1-D cross-over contour (the bold line in the bottom panel) starting from the western edge. The bars above the velocity profile display the traveltime variation, each bar marking the point where S_{ab} is 0.5 earlier than its western neighbour. Dense bar spacings indicate a strong transverse velocity gradient and thus stronger 3-D effects. (b) Equidifferential time contours, where the differential is $S_{ab} - S_{cd}$. The numbers -4, -2, 0, 2, 4 and 6 are the differential times in seconds. The background is the velocity profile of the basal layer near the CMB from Grand's model.

of Fig. 14, a contour map indicating the position of cross-over (heavy line) is displayed along with timing lines. These curves indicate the separation between the two arrivals, S_{ab} and S_{cd}, as displayed in Fig. 2. Mapping cross-over distance has the advantage of excluding the upper mantle effects, since S_{cd} ray paths and S_{ab} ray paths are very close together in the upper mantle. If the lower mantle velocity structure is 1-D, the cross-over distance should be equal along different azimuths. Thus, the deviation of cross-over contours from a circle implies lateral variation in the lower mantle velocity structure, which is easily observable with a deviation of about about 1° in this case. The pattern changes most rapidly along the eastern edge of Grand's Caribbean anomaly, as shown.

The upper portion of Fig. 14 displays a cross-section across the North America continent, roughly along the cross-over contour. The triangles indicate the azimuth appropriate to EDM and FBC with the event in South America. The path passing through the upper mantle to EDM is thus clearly tectonic (TNA) relative to FBC (SNA). The bars indicate traveltime steps in intervals of 0.5 s that are appropriate for the upper mantle contribution to traveltimes along the cross-over lines. The relative changes between S_{ab} and S_{cd} for the whole paths are considerably reduced because of the compensating effects discussed earlier.

4 DISCUSSION AND CONCLUSIONS

The 2-D synthetics predicted from a modified Grand model show amplitude variation and differential traveltime variations, similar to all S_{cd} modelling attempts. However, as discussed in the Introduction, the lower mantle is 3-D. This puts doubts on the validity of 2-D modelling. If the velocity gradients are small enough or if the velocity does not vary by more than a few per cent in one wavelength, 2-D modelling should be adequate. There are some *a posteriori* criteria to test the validity of 2-D modelling. If the 2-D synthetics do not change much for a small change in azimuth, it appears that the 2-D modelling is applicable. An example of this situation can be seen in Fig. 14, where the bar spacing indicates rapid lateral traveltime variations. Dense bars imply strong variation, and whilst the transition from TNA to SNA is interesting, studying deep Earth structure near this transition boundary is probably risky. In short, the earth is 3-D, but judiciously chosen 2-D sections should prove useful in mapping these structures.

Another limitation of our method occurs when the structures have sharp features. For example, in the study of TERRAscope data, we can begin to see rapid variations in the timing and shapes of S_{cd}. TRINET (Jones *et al.* 1999) is increasing the station density tenfold, which will undoubtedly provide such data, and the many existing or planned PASCAL experiments will also increase the data available. Sharp features in the presence of strong velocity contrasts will produce diffraction effects that are not handled with this approximation. However, since the waveform solution can be decomposed into individual rays (dp_i/dt_i), they can be shifted and reassembled to simulate neighbouring models as in Song & Helmberger (1998). The inverse problem can be effectively addressed and structures defined. Complete wavefields from such structures can be produced by more sophisticated codes such as those discussed in Wen & Helmberger (1998).

In conclusion, we developed a useful method of constructing 2-D synthetics for tomography models. The method is related to a modification of WKBJ, hence the name WKM. However, it is basically a first-motion approximation of generalized ray theory and is compatible with Cagniard–de Hoop methods. This feature makes it attractive for studying structures with large velocity jumps near the CMB, and shadow-zone boundaries. An application of the method to Grand's tomography model proved quite successful in explaining some of the S_{cd} behaviour observed for the D″ structure beneath central America. The technique is presently being used to study the low-velocity structures beneath Africa and will be reported on soon.

ACKNOWLEDGMENTS

This project was supported by the National Science Foundation grant number EAR97-2508. We thank the two anonymous reviewers for their comments, which helped to improve this paper. We also thank Mike Gurnis for his helpful suggestions. Contribution number 8631 of the Division of Geological and Planetary Sciences, California Institute of Technology.

REFERENCES

Aki, K. & Richards, P.G., 1980. *Quantitative Seismology Theory and Methods,* Vol. 1, W.H. Freeman, San Francisco.

Breger, L. & Romanowicz, B., 1998. Three-dimensional structure at the base of the mantle beneath the central pacific, *Science,* **282,** 718–720.

Breger, L., Romanowicz, B. & Vinnik, L., 1998. Test of tomographic models of D″ using differential travel time data, *Geophys. Res. Lett.,* **25,** 5–8.

Burdick, L.J. & Salvado, C.A., 1986. Modeling body wave amplitude fluctuations using the three-dimension slowness method, *J. geophys. Res.,* **91,** 12 482–12 496.

Chapman, C.H., 1976. Exact and approximate ray theory in vertically inhomogeneous media, *Geophys. J. R. astr. Soc.,* **6,** 201–233.

Chapman, C.H., 1978. A new method for computing synthetic seismograms, *Geophys. J. R. astr. Soc.,* **56,** 81–85.

Chapman, C.H. & Drummond, R., 1982. Body-wave seismograms in inhomogeneous media using Maslov asymptotic theory, *Bull. seism. Soc. Am.,* **72,** 277–237.

Chapman, C.H. & Orcutt, J.A., 1985. The computation of body wave synthetic seismograms in laterally homogeneous media, *Rev. Geophys.,* **23,** 105–163.

Ding, X., Helmberger, D.V., 1997. Modeling D″ Structure with broadband seismic data, *Phys. Earth. planet. Inter.,* **101,** 245–270.

Dziewonski, A.M. & Anderson, D.L., 1981. Preliminary reference Earth model, *Phys. Earth. planet. Inter.,* **25,** 297–356.

Frazer, L.N. & Phinney, R.A., 1980. The theory of finite frequency body wave synthetic seismogram in inhomogeneous elastic media, *Geophys. J. R. astra. Soc.,* **63,** 691–713.

Gilbert, F. & Helmberger, D.V., 1972. Generalized ray theory for a layered sphere, *Geophys. J. R. astra. Soc.,* **27,** 57–80.

Grand, S.P., 1994. Mantle shear structure beneath the Americas and surrounding oceans, *J. geophys. Res.,* **99,** 11 591–11 622.

Grand, S.P. & Helmberger, D.V., 1984. Upper mantle shear structure of North America, *Geophys. J. R. astra. Soc.,* **76,** 399–438.

Graves, R.W & Helmberger, D.V., 1988. Upper mantle cross section from Tonga to Newfoundland, *J. geophys. Res.,* **93,** 4701–4711.

Helmberger, D.V., 1968. The crust-mantle transition in the Bering Sea, *Bull. seism. Soc. Am.,* **58,** 179–214.

Helmberger, D.V., Zhao, L.S. & Garnero, E.J., 1996. Construction of synthetics for 20 structures: core phases, in *Seismic Modeling of Earth Structure,* pp. 183–222, eds Boschi, E., Ekstrom, G. & Morelli, A., North-Holland, New York.

Hong, T.L. & Helmberger, D.V., 1978. Glorified optics and wave

propagation in nonplanar structure, *Bull. seism. Soc. Am.,* **68,** 1313–1330.

Jones, L.M. *et al.,* 1999. *Modern digital, multifunctional real time seismographic network for southern California, US: TRINET,* IUGG, Birmingham, pp. 18–30.

Kendall, J.-M. & Nangini, C., 1996. Lateral variations in D″ below the Caribbean, *Geophys. Res. Lett.,* **19,** 399–402.

Lay, T. & Helmberger, D.V., 1983. A lower mantle S-wave triplication and the shear velocity structure of D″, *Geophys. J. R. astr. Soc.,* **75,** 799–838.

Lay, T., Williams, Q. & Garnero, E.J., 1998. The core-mantle boundary layer and deep Earth dynamics, *Nature,* **392,** 461–468.

Liu, X.F. & Tromp, J., 1996. Uniformly valid body-wave ray theory, *Geophys. J. Int.* **127,** 461–491.

Liu, X.F., Tromp, J. & Dziewonski, A.M., 1998. Is there a first-order discontinuity in the lowermost mantle?, *Earth planet. Sci. Lett.,* **160,** 343–351.

Ni, S., Ding, X. & Helmberger, D.V., 1999. Low-velocity structure beneath Africa from forward modeling, *Earth planet. Sci. Lett.,* **170,** 497–507.

Sidorin, I. & Gurnis, M., 1998. Geodynamically consistent seismic velocity predictions at the base of the mantle, in *Structure, Composition, and Dynamics of the Core-Mantle Boundary Region,* pp. 273–297, eds Gurnis, M., Wysession, M., Knittle, E. & Buffett, B., AGU, Washington.

Sidorin, I., Gurnis, M., Helmberger, D. & Ding, X, 1998, Interpreting D″ seismic structure using synthetic waveforms computed from dynamic models, *Earth planet. Sci. Lett.,* **163,** 31–41.

Song, X.J. & Helmberger, D.V., 1998. Pseudo Green's functions and waveform tomography, *Bull. seism. Soc. Am.,* **88,** 304–312.

Su, W.-J., Woodward, R.L. & Dziewonski, A.M., 1994. Degree 12 model of shear velocity heterogeneity in the mantle, *J. geophys. Res.,* **99,** 6945–6980.

Vidale, J. & Helmberger, D.V., 1988. Elastic finite-difference modeling of the 1971 San-Fernando, California earthquake, Bull. seism. Soc. Am., **78,** 122–141.

Wahba, G., 1990. Spline models for observational data, in *CBMS-NSF Regional Conference Series in Applied Mathematics,* Vol. 59, pp. 45–52, Society for Industrial and Applied Mathematics, Philadelphia.

Weber, M., Davis, J., Peter, C.T., Krueger, F., Scherbaum, F., Schlittenhardt, J. & Koernig, M., 1996. The structure of the lowermost mantle as determined from using seismic arrays, in *Seismic Modeling of Earth Structure,* pp. 183–222, eds Boschi, E., Ekstrom, G. & Morelli, A., North-Holland, New York.

Wen, L.X. & Helmberger, D.V., 1998. Ultra-low velocity zones near the core-mantle boundary from broadband PKP precursors, *Science,* **279,** 1701–1703.

Wiggins, R.A., 1976. Body wave amplitude calculations, II, *Geophys. J. R. astr. Soc.,* **46,** 1–10.